


Modeling Fischer–Tropsch kinetics and product distribution over a cobalt catalyst

Umesh Pandey¹ | Anders Runnengen¹ | Ljubiša Gavrilović¹ | Erik A. Jørgensen¹ |
Koteswara R. Putta¹ | Kumar R. Rout^{1,2} | Erling Rytter^{1,2} | Edd A. Blekkan¹ |
Magne Hillestad¹ 

¹Norwegian University of Science and Technology, Trondheim, Norway

²SINTEF Industry, Norway

Correspondence

Magne Hillestad, Norwegian University of Science and Technology, 7491, Trondheim, Norway.

Email: magne.hillestad@ntnu.no

Funding information

Norges Forskningsråd

Abstract

A detailed kinetic model describing the consumption of key components and product distribution in the Fischer–Tropsch synthesis (FTS) over a 20%Co/0.5Re γ -Al₂O₃ commercial catalyst is developed. The developed model incorporates the H₂O-assisted CO dissociation mechanism developed by Rytter and Holmen and a novel approach to product distribution modeling. The model parameters are optimized against an experimental dataset comprising a range of process conditions: total pressure 2.0–2.2 MPa, temperature 210–230 °C, CO conversion range of 10%–75% and feed with and without added water. The quality of the model fit measured in terms of mean absolute relative residuals (MARR) value is 23.1%, which is comparable to literature reported values. The developed model can accurately describe both positive and negative effects of water on the rate kinetics, the positive effect of water on the growth factor, temperature and syngas composition on the kinetics and product distribution over a wide range of process conditions, which is critical for the design and optimization of the Fischer–Tropsch reactors.

KEYWORDS

Fischer–Tropsch, mathematical modeling, reaction kinetics

1 | INTRODUCTION

Rising world energy demand and possible future stringent regulation on fossil fuel exploration due to their role in climate crisis have unlocked exciting new opportunities for renewable energy resources. Advanced biofuels production via gasification of biomass and subsequent Fischer–Tropsch synthesis (FTS) is a promising alternative fuel solution since the substitute fuel can utilize existing infrastructure. Besides, the fuel has similar characteristics as its conventional alternatives (fossil-based jet and diesel fuel), including a high energy density and storability, thus making it one of the best alternatives for aviation and long-haul transportation.

FTS is a surface polymerization reaction of CO and H₂ producing higher hydrocarbons, traces of oxygenated products as well as H₂O and CO₂. The hydrocarbon product predominantly contains n-paraffins and 1-olefins, but the distribution of products depends on the process condition along with the type of catalyst and physical characteristics of the catalyst.^{1,2} The FTS can be broadly categorized into two types: high temperature (300 – 350 °C) Fischer–Tropsch (HTFT) synthesis over catalysts active for the water-gas shift reaction such as iron-based catalysts, and low temperature (200 – 240 °C) Fischer–Tropsch (LTFT) synthesis over non-shifting catalysts such as cobalt catalysts.^{3,4} Among these two types of FTS, the LTFT over cobalt catalyst is of primary interest in the present work as the

This is an open access article under the terms of the Creative Commons Attribution-NonCommercial-NoDerivs License, which permits use and distribution in any medium, provided the original work is properly cited, the use is non-commercial and no modifications or adaptations are made.

© 2021 The Authors. *AIChE Journal* published by Wiley Periodicals LLC on behalf of American Institute of Chemical Engineers.

product from LTFT has a higher paraffin fraction, which is suitable for the jet/diesel fuel. Besides, the cobalt catalysts have higher activity, allowing for commercially interesting conversion in reasonable reactor volumes at low temperature, and the cobalt catalyst used in the LTFT is more stable with respect to deactivation than iron catalysts used in the HTFT.⁵ Currently, gas to liquid technology (GtL)⁶ and coal to liquid technology (CtL),³ which incorporates natural gas/coal gasification and FTS, are commercially available. The adaptation of GtL/CtL technologies to biomass to liquid (BtL) technology with biomass as a feed is an attractive option for low carbon future. However, the development of industrial BtL plants, as well as GtL and CtL plants, are dependent on the understanding of the FT kinetics and product distribution as it is essential for the design and scale-up of the FT reactors.

FTS has been around for several decades, and multiple attempts have been made to describe the FT reaction mechanism and product distributions.^{5,7-15} In general, four different mechanisms can be found in the literature: carbide mechanism,^{5,8,11} enol mechanism,¹¹ CO-insertion mechanism^{11,13,14} and hydrogen assisted CO activation.^{12,16-18} In the carbide mechanism, the formation of CH_x species is facilitated by the dissociation of C – O bonds on the catalyst surface.² The carbide mechanism was first proposed by Fischer and Tropsch¹⁹ and is widely considered the primary mechanism in the HTFT synthesis. Some authors reported it as a primary mechanism for LTFT synthesis.^{5,8,11} In the CO-insertion mechanism, the chain growth takes place by direct insertion of CO into the metal alkyl bond.^{2,13,14} In the enol mechanism, it has been suggested that CO gets directly adsorbed to form oxygenates (enol species) which are responsible for the chain growth in FTS.²⁰ The hydrogen assisted CO activation proceeds via $^*\text{CHO}$ (formyl) and $^*\text{CH}_2\text{O}$ and dissociation to CH_2 and O. This activation step was further developed by Rytter and Holmen in the water-assisted CO dissociation mechanism where the oxygen atom in formyl (or in $^*\text{CH}_2\text{O}$) is abstracted by a hydrogen atom coming from water or hydroxyl.⁷ This explains the often-observed effect that the FT rate increases with increasing water vapor pressure.

There are three crucial steps in the kinetic modeling of the FTS: (a) identification of the plausible mechanism, (b) formulating the consumption rate of the primary component CO, and (c) describing the product distribution. Most of the published literature on kinetic studies of the FTS developed Langmuir–Hinshelwood–Hougen–Watson (LHHW) kinetic rate expressions for surface polymerization reaction,^{5,7-15} or simple power-law expression and fitted against experimental data.²¹⁻²³ The primary focus of most of these studies is formulating rate equation for CO consumption while many of them have incorporated detailed product modeling in their kinetic studies.^{5,7,9,10,13-15,22,23} The LHHW kinetic expressions published in the literature have model structure encompassing the partial pressures of hydrogen and CO, p_{H_2} and p_{CO} .^{5,7-14,21-24} Only a handful of published kinetic studies incorporated water effects²⁵⁻²⁹ and this needs further attention as water is a key component in the FTS. Rytter and Holmen derived an LHHW kinetic expression embodying both positive and negative effects of water on the FT rate.⁷

Many of the published models attempted to describe product distribution using ideal Anderson-Schulz-Flory (ASF) distribution^{5,7,9,10,13-15,22,23} while; recently, Sun et al³⁰ formulated an artificial neural networks—response surface methodology approach to product distribution modeling.

The former approach is of primary interest as the latter approach lacks two critical qualities of physical modeling: generalization and physical interpretation. In the cases of ASF distribution based product modeling, α was usually modeled as a function of p_{H_2} and p_{CO} .^{5,13,14,31-33} A recent experimental investigation on FTS showed that water has both positive and negative effects on the CO consumption rate and has a positive effect on the chain growth probability.³⁴ In addition, Oosterbeek and Bavel experimentally verified that p_{H_2} does not affect growth probability.³⁵ This is possible only if adsorbed hydrogen is responsible for both chain propagation and chain termination. The published models fail to address this critical information as almost all the published model have incorporated p_{H_2} in the growth model. In addition, the effect of water on the α is well documented in the literature although only a handful of the recent kinetic studies have incorporated water effects in the α model.^{13,14,36} One of the critical issues in product distribution modeling of the FTS based on the ASF distribution is how to describe the rate of formation of paraffin and olefins in the FTS. Earlier attempts of product modeling by Pannell et al²² and Wojciechowski et al⁹ and Yang et al²³ focused on describing overall product distribution without much emphasis on the olefin-paraffin distribution. Many of the recently published kinetic studies have tried to formulate separate polymerization reactions for olefins and paraffin.^{13-15,25,36} The common assumption in most of these studies is that there are two different sites for the polymerization reaction with two different growth probabilities: one for olefins and another for paraffin. However, a recent study by Rytter et al shows that olefins are primary products and are not independent of the paraffin formation reaction.³⁷ Besides, existing kinetic models fail to describe the independent characteristics of hydrogen partial pressure p_{H_2} on the growth probability. Rytter and Holmen incorporated these pieces of evidence and proposed H_2 assisted CO dissociation mechanism, which suggests that olefins are the primary product and paraffin are formed as secondary products.⁷ Thus, it is possible to describe the overall polymerization reaction using ASF distribution with a single growth probability as a distribution parameter and formulate a separate distribution to describe olefins and paraffin, which is implemented in the present work.

Furthermore, the product distribution deviates from the ASF distribution, which is well documented in the literature.^{33,38-40} The deviations arise from the process conditions such as a change in pressures, temperatures, and composition.^{33,39} However, the process deviation is much smaller than the inherent deviation in the FTS: substantially higher selectivity to methane, and lower selectivity to ethylene⁴¹ in comparison to the selectivities based on the ideal ASF distribution. Most of the published kinetic studies introduced separate rate constants for methane and ethylene formation, which is often different from the primary FT reaction to describe the non-ASF distribution of methane and ethylene in the product.^{13-15,17,41} They proposed a separate reaction for methane formation speculating methanation occurs on a different catalytic site^{42,43} or via a different mechanism.⁴⁴ However, this is in direct contradiction to experimental observations reported by Rytter and Holmen.³⁷ They reported that methane formation is not independent of the primary FT-polymerization reaction, which implies that any future attempts toward methane product modeling must not deviate from the

primary polymerization reaction. In the case of ethylene, kinetic studies assumed that the lower selectivity of ethylene due to the particular characteristics of the ethylene; re-adsorption of the ethylene species.^{13,14,17,23,25,41} However, Withers et al²⁹ studied the effect of adding ethylene in the feed (10–20%wt) and reported that additional ethylene increased ethane and oxygenates formation without much change in other product formation rates.²⁹ This shows that ethylene re-adsorption has little or no impact on the overall product distribution.

In general, there are four critical shortcomings in the literature published models. They fail to (a) address the effect of water on the CO consumption rate and product distribution, (b) independency of p_{H_2} on growth probability, (c) olefin/paraffin product distribution, and (d) deviation in methane and ethylene selectivities. Rytter and Holmen⁷ proposed a hydrogen assisted kinetic mechanism, which addressed the first three shortcomings. The present work formulates a predictive kinetic model based on the mechanism proposed by Rytter and Holmen⁷ which can mechanistically describe the effect of water, temperature and composition of key components on reaction rate, olefin-paraffin distribution, and catalyst deactivation modeling covering most of the critical aspects of FTS over the cobalt catalyst. Three separate reactions as a function of primary polymerization reaction are introduced to address deviation from the ASF distribution in the methane and ethylene selectivities which aims to incorporate recent pieces of evidence on the FTS as reported in the literature.^{18,37}

Furthermore, the model formulation applied here is “closed” in the sense that the infinite number of reactions and species are lumped such that all elements are conserved. The product distribution, including the C_{5+} paraffin and olefin, are modeled and follow the Anderson–Schulz–Flory distribution. Deviations from the ASF distribution are taken into account. All measured responses, the total CO consumption, and all measured product formations are used when the kinetic model is regressed. This is an entirely different approach compared to some of the published kinetic models as they have either fitted selective components^{9,13,14} or olefins to paraffin ratio of selective components⁵ in their kinetic modeling and failed to account the production of higher components.

2 | CO CONSUMPTION RATE AND PRODUCT DISTRIBUTION MODELING

2.1 | CO consumption rate modeling

Various CO consumption rate equations are published in the literature. Most of them can be generalized based on LHHW kinetic expressions, as shown in Equations (1) and (2).^{5,7-14,21-24} The best model structure was then reported based on the model performance against the experimental observations.^{5,7-15} In other cases, simple power-law equations were fitted against experimental observations.²¹⁻²³ A summary of literature published rate equations can be found elsewhere.^{15,27,36}

$$r_{FT} = \frac{kp_{CO}^{m_1} p_{H_2}^{m_2}}{\left(1 + \sum_i K_i p_{CO}^{j_i} p_{H_2}^{l_i}\right)^2} \quad (1)$$

$$k = k_{ref} e^{-\frac{E_a}{R} \left(\frac{1}{T} - \frac{1}{483}\right)} \quad (2)$$

Equation (1) does not contain the effect of water, while some of the literature published models have incorporated the effect of water, as shown in Equation (3).²⁵⁻²⁹

$$r_{FT} = \frac{kp_{CO}^{m_1} p_{H_2}^{m_2} p_{H_2O}^{m_3}}{\left(1 + \sum_i K_i p_{CO}^{j_i} p_{H_2}^{l_i} p_{H_2O}^{k_i}\right)^2} \quad (3)$$

An LHHW expression shown in Equation (4), similar in characteristic to Equation (3), developed by Rytter and Holmen⁷ based on the consorted vinylene mechanism, was considered in the present work. In this CO consumption model, water plays two different contrasting roles in the primary polymerization reaction: positive effect due to its role in H_2O assisted CO dissociation and negative effect due to surface covering of active catalyst sites by water molecules.⁷ In Equation (4), $dp_{CO} p_{H_2}^{1/2} / p_{H_2O}$ represents the former activation effect, while $f p_{H_2O} / p_{H_2}^{1/2} + g p_{H_2O}$ represents the latter effect where the f -term relates to hydroxyl surface coverage and the d term to water activation.

$$r_{FT} = \frac{kp_{CO} p_{H_2}^{1/2}}{\left(1 + (a+c)p_{CO} + b p_{H_2}^{1/2} + d \frac{p_{CO} p_{H_2}^{1/2}}{p_{H_2O}} + e p_{CO} p_{H_2}^{1/2} + \frac{f p_{H_2O}}{p_{H_2}^{1/2}} + g p_{H_2O}\right)^2} \quad (4)$$

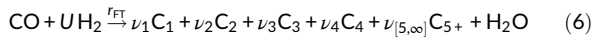
In the non-linear model fitting, it turned out impossible to statistically identify the two terms, $f p_{H_2O} / p_{H_2}^{1/2}$ and $g p_{H_2O}$, that represent the same negative effect on the reaction rate with water vapor pressure due to strong covariance between the coefficients, f and g . Similarly, the adsorption coefficient e , representing hydroxycarbene (HCOH) in the surface,⁷ is strongly correlated to $(a+c)$. Additionally, HCOH is assumed to be present in only minor amounts, and the e term is therefore neglected in further analysis. Upon further investigation, it revealed that d term in the model introduces a numerical singularity as p_{H_2O} is zero at the reactor inlet. Furthermore, this causes numerical stiffness in the differential equations. These numerical limitations are addressed by simplifying the model, as shown in Equation (5). In the simplified equation, a' represents the combined effects of a , c , & e , and f' represent combined effects of f & g or the negative effect of water. A term, $k_{p_{H_2O}} p_{H_2O}$, is introduced in the numerator to account for the positive effect of water instead of $dp_{CO} p_{H_2}^{1/2} / p_{H_2O}$ term in the denominator as in Equation (4).

$$r_{FT} = \frac{kp_{CO} p_{H_2}^{1/2} \left(1 + k_{p_{H_2O}} p_{H_2O}\right)}{\left(1 + a' p_{CO} + b p_{H_2}^{1/2} + f' p_{H_2O}\right)^2}; \quad k_{p_{H_2O}} = 0.1 \text{ MPa}^{-1} \quad (5)$$

2.2 | Modeling product distribution

2.2.1 | Growth probability and ASF distribution

The product distribution between HCs of different chain lengths can be described by Anderson-Schultz-Flory (ASF) distribution. The name derives from the work of R.B. Anderson. He modified the Flory-Schulz equation, commonly used to describe the molecular distribution of the polymerization reaction at the time, to describe the FT product distribution.⁴⁵ Early work in this area mostly consisted of describing total HCs distribution with specific carbon chain length without much emphasis on the olefins-paraffin distribution. In recent years, an effort is devoted to explaining olefins and paraffins distribution separately. Two growth probabilities, one for olefins and another for paraffins is speculated in the literature^{46,47} and later incorporated as a part of mechanistic or semi-empirical product distribution modeling.^{13,14,36} Todici et al^{13,14} fitted a constant ratio between the growth factors, which was subsequently incorporated by Ostadi et al³⁶ in their modeling of product distribution. In the present work, we considered Consorted Vinylene Mechanism which proposed that olefins are formed as primary products (C_i) and follow the Anderson-Schultz-Flory distribution.⁷



The modeling of Anderson-Schultz-Flory distribution; determination of stoichiometric coefficients (ν_i), hydrogen utilization ratio (U), average carbon number in the lump ($\bar{N}_{[i,\infty]}$) and stoichiometric coefficient of the lump ($\nu_{[5,\infty]}$) as a function of the chain length (i) and growth probability (α) are formulated by Hillestad.⁴⁸

$$\nu_i = (1-\alpha)^2 \alpha^{i-1} \quad (7)$$

$$\nu_{[n,\infty]} = (1-\alpha) \alpha^{n-1} \quad (8)$$

$$\bar{N}_{[n,\infty]} = n + \frac{\alpha}{1-\alpha} \quad (9)$$

$$U = 3 - \alpha \quad (10)$$

The hydrogen utilization ratio defined in Equation (10) is for paraffin only. The growth probability (α) is described in terms of the rate of propagation (r_p) and the rate of termination (r_T) as shown in Equation (11).

$$\alpha = \frac{r_p}{r_p + r_T} \quad (11)$$

Various empirical or semi-empirical models for α can be found in the literature.^{13,14,31,32,36} The literature published α -model mostly considered the effect of p_{H_2} and p_{CO} in their growth probability model.

Experimental pieces of evidence showed that the selectivity to C_{5+} increases with the partial pressure of water.^{34,49} Most of the published models fall short of explaining the effect of the partial pressure of water on product distribution. Ostadi et al³⁶ fitted an empirical form of the growth model, including partial pressure of water, as shown in Equation (12).

$$\alpha = \frac{1}{1 + k_\alpha(T_k) \frac{p_{\text{H}_2}^n}{p_{\text{CO}}^m p_{\text{H}_2\text{O}}^p}} \quad (12)$$

Nevertheless, the growth model fitted by Ostadi et al³⁶ failed to incorporate the independency of p_{H_2} on growth probability as reported by Oosterbeek and Bavel.³⁵ This revelation was later incorporated by Rytter et al in the Consorted Vinylene Mechanism.⁷ The mechanism suggests that p_{H_2} is involved in both termination and propagation of the carbon chain; thus, it is possible to exclude p_{H_2} from the growth model and was considered in the present work, as shown in Equation (13).

$$\alpha = \frac{1}{1 + k_\alpha(T_k) \frac{1}{p_{\text{CO}}^m p_{\text{H}_2\text{O}}^p}} \quad (13)$$

From Equation (11), it shows that k_α is the ratio between two rate constants. Therefore, k_α will follow Arrhenius type equation but simplified as we may have more than one termination reaction. In general, activation energy (E_α^a) is positive as the termination increases faster with the temperature than the propagation, which is also reported in the literature.^{9,22,31,37}

$$k_\alpha = k_{\alpha,\text{ref}} e^{-\frac{E_\alpha^a}{R} \left(\frac{1}{T} - \frac{1}{483} \right)} \quad (14)$$

2.2.2 | Olefins-paraffin distribution

In the Consorted Vinylene mechanism considered in the present work, primary olefin products (C_i) are either converted to paraffin (C_i^p) or desorbed as olefins (C_i^o) incorporated in the final products. A probabilistic distribution can describe the distribution of b_i , where b_i is the probability of olefins formation.

$$C_i^o = b_i C_i \quad (15)$$

$$C_i^p = (1 - b_i) C_i \quad (16)$$

The probability of olefin formation decreases with chain length,^{31,50} so, it is possible to define a probabilistic distribution as a function of chain length (i) and distribution parameter (β).

$$b_i = \beta^{i-1} \quad (17)$$

The probabilistic distribution of olefins and paraffin with $\beta = 0.8$ is shown in Figure 1. It shows decreasing olefins production and increasing paraffin production with chain length. This is also what is observed in the FTS.

For the modeling of the probabilistic distribution parameters, β , it is essential to understand the characteristics of olefins paraffins ratio with the variation in process parameters. It is reported in the literature that olefins to paraffin ratios depend on the partial pressures of CO,^{34,51} H₂⁵¹ and temperature.^{37,51-53} Rytter et al also reported increased olefins to paraffin ratio with water addition.³⁴ Based on these pieces of evidence, a semi-empirical model, as shown in Equation (18), was considered for β model.

$$\beta = \frac{1}{1 + \frac{k_{\beta}(T_k) p_{H_2}^{x_1}}{p_{CO}^{x_1} p_{H_2O}^{x_2}}} \quad (18)$$

Preliminary model fitting shows that olefins hydrogenation to paraffins strongly depends on the residence time in the reactor and is weakly dependent on other process variables such as p_{H_2} and p_{H_2O} . Recently, Rytter et al also reported a strong negative effect of residence time on olefins to paraffins ratio along with the weak effect of p_{H_2O} and p_{H_2} ⁵⁴ indicating that residence time plays a major role in the olefin-paraffin product distribution. The residence time in the FTS is strongly correlated with the conversion or decrease in the p_{CO} ; thus, a simple β -model explaining the effect of residence time is proposed for describing hydrogenation of primary olefin to paraffin. The model also indirectly incorporates an increase in the hydrogenation of olefins to paraffin with increasing H₂ pressure in the reactor.

$$\beta = \frac{1}{1 + \frac{k_{\beta}(T_k)}{p_{CO}}} \quad (19)$$

Here, the Arrhenius type equation was considered for k_{β} to explain increasing paraffin fraction with temperature as reported in the literature.^{37,52,53}

$$k_{\beta} = k_{\beta,ref} e^{-\frac{E_{\beta}}{R} \times \left(\frac{1}{T_k} - \frac{1}{483} \right)} \quad (20)$$

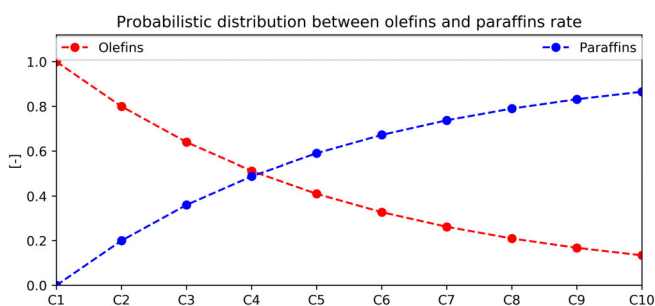
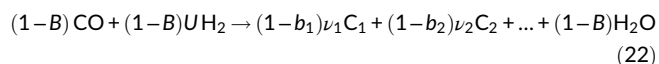
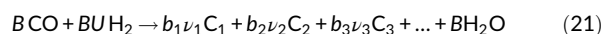


FIGURE 1 Probabilistic distribution of olefins and paraffins rate. Here C1, methane, is counted among the olefins as well as the paraffins [Color figure can be viewed at wileyonlinelibrary.com]

2.3 | Summary of overall product distribution

The product distribution modeling proposed here can be summarized, as shown in Figure 2. The schematics show probabilistic distribution of olefins and paraffin and stepwise chain growth mechanism as a function of two distribution parameters; α and β .

For modeling purposes, it is possible to formulate two overall reactions, one for paraffins and another for olefins by integrating ASF distribution (Equation (6)) and olefins-paraffins distribution (Equations (15–17)), as shown in Equations (21 and 22).



The carbon balance gives,

$$B = \frac{(1-\alpha)^2}{(1-\alpha\beta)^2} \quad (23)$$

Here, the overall olefins rate is $r_{FT}^O = B r_{FT}$, while the paraffin rate is $r_{FT}^P = (1-B) r_{FT}$. The overall rate in terms of unitized CO consumption can be summarized as shown in Equations (24) and (25), for olefins and paraffins, respectively.

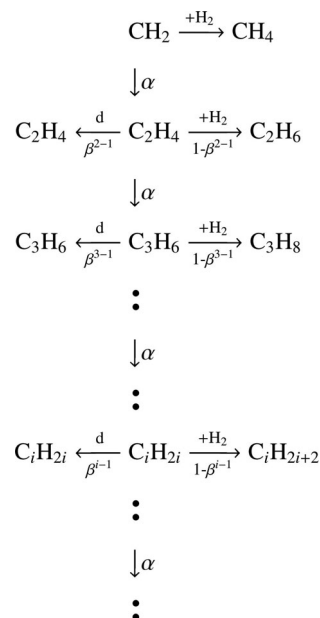
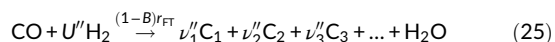
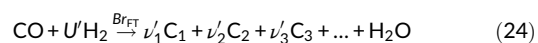


FIGURE 2 Schematics of stepwise chain growth and olefins-paraffin distribution based on the proposed model

The overall reaction for olefins formation is identical to the ideal ASF distribution with the growth parameter as $\alpha\beta$. The stoichiometric coefficients (ν'_i), average carbon number in the lump ($N'_{[i,\infty]}$), and stoichiometric coefficient of the lump ($\nu'_{[5,\infty]}$) as a function of the chain length (i) and growth probability ($\alpha\beta$) can be formulated, as shown in Equations (7)–(10). The H_2 consumption rate for the overall olefins reaction can be formulated, as shown in Equation (26).

$$U' = 2 + (1 - \alpha\beta)^2 \quad (26)$$

In the case of paraffins, the stoichiometric coefficients (ν''_i) and hydrogen usage rates (U'') for overall paraffins formation reaction can be derived using the sum of stoichiometric coefficients, as shown in Equations (27) and (28).

$$\nu''_i = \frac{1}{1-B} \left[(1-\alpha)^2 \alpha^{i-1} - (1-\alpha)^2 (\alpha\beta)^{i-1} \right] \quad (27)$$

$$U'' = 2 + \frac{1-\alpha}{1-B} \left(1 - \frac{1-\alpha}{1-\alpha\beta} \right) \quad (28)$$

The tail component of the paraffin can be lumped to a single lump component. The tail lump stoichiometric coefficient ($\nu''_{[i,\infty]}$) and the average number of carbon in the chain length ($N''_{[i,\infty]}$) for the paraffin lumps can be calculated as shown in Equations (29) and (30), respectively.

$$\nu''_{[i,\infty]} = \frac{1}{1-B} (1-\alpha) \alpha^{i-1} \left[1 - \frac{\beta^{i-1} (1-\alpha)}{1-\alpha\beta} \right] \quad (29)$$

$$\bar{N}''_{[i,\infty]} = \frac{\left[\frac{\alpha^{i-1} (\alpha - i\alpha + i)}{(1-\alpha)^2} - \frac{(\alpha\beta)^{i-1} (\alpha\beta - i\alpha\beta + i)}{(1-\alpha\beta)^2} \right]}{\left[\frac{\alpha^{i-1}}{1-\alpha} - \frac{(\alpha\beta)^{i-1}}{(1-\alpha\beta)} \right]} \quad (30)$$

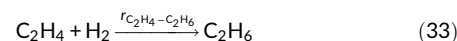
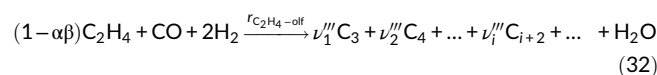
2.4 | Anomaly from the ideal distribution

The ideal distribution discussed here cannot explain the higher selectivity of methane and lower than expected selectivity of ethylene. For practical reasons, methane is modeled as a separate methanation reaction. Rytter et al have experimentally verified that methane selectivity is not independent of the growth model, although, observed methane formation is substantially higher than the ideal ASF distribution.³⁷ Besides, the study showed that methane formation increases with p_{H_2} .⁵⁵ These observations were addressed in the present work by introducing a methanation reaction which is a function of ideal product distribution and p_{H_2} , as shown in Equation (31). Here, $r_{CH_4,ideal}$ is the total methane formation based on the ideal distribution.

$$r_{CH_4} = k_{CH_4} r_{CH_4,ideal} p_{H_2} \quad (31)$$

In the case of ethylene, the lower selectivity is primarily due to the lower stability of ethylene intermediary species due to the lower

activation energy or higher enthalpy of formation of the ethylene species compared to higher olefins.⁴¹ Due to this fact, a significant fraction of ethylene supposed to be formed based on ASF distribution either gets converted to ethane or polymerizes to give higher olefins. Two separate reactions describing the conversion of a fraction of ethylene to ethane ($r_{C_2H_4-C_2H_6}$) and ethylene to higher chain olefins ($r_{C_2H_4-olf}$), is proposed to explain lower than expected selectivity to ethylene. In the former reaction, it is assumed that ethylene is secondarily hydrogenated to ethane. This assumption is supported by the study by Withers et al,²⁹ where they reported that adding 10–20 weight% ethylene in the feed increased ethane and oxygenates products without much change in other products. In the latter reaction, it is assumed that ethylene intermediates are further polymerized without desorption of the freshly formed ethylene species. The product distribution for the apparent polymerization of ethylene follows ASF distribution and is given by Equations (7)–(10). The growth probability of this apparent reaction is identical to the growth probability for overall olefin formation reaction, $\alpha\beta$. Equations (32–35) shows the modeling of ethylene conversion to ethane and higher olefins.



$$r_{C_2H_4-C_2H_6} = k_{C_2H_4-C_2H_6} r_{C_2H_4,ideal} \quad (34)$$

$$r_{C_2H_4-olf} = k_{C_2H_4-olf} \frac{r_{C_2H_4,ideal}}{1-\alpha\beta} \quad (35)$$

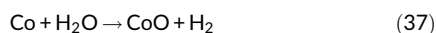
2.5 | Deactivation modeling

Deactivation captures the transient effect of the process, mainly catalyst deactivation and its impact on the overall FTS. As Tsakoumis et al⁵⁶ pointed out, catalyst deactivation is a complex issue that occurs via several mechanisms: poisoning by the formation of sulfurous and nitrogenous compounds, sintering, coke deposition, carbide formation and re-oxidation of catalyst. The re-oxidation occurs in the presence of water and causes a substantial increase in the catalyst deactivation, which is facilitated by high CO conversion or water in the feed. The effect of water in catalyst deactivation was reported by Dalai and Davis⁵⁷ and Storsæter et al.⁴⁹ It was suggested that a permanent deactivation of Co catalyst occurs at a high partial pressure of water due to the formation of inactive Co(II) oxide or support collapse. A second-order deactivation model (Equation (36)), along with the effect of water on the deactivation, was considered in the present work. Besides, the partial pressure of water in the deactivation model also addresses other modes of deactivation; as higher partial pressure of water mostly indicates higher CO conversion or higher temperature induced from the higher CO conversion. These events ultimately lead

to catalyst deactivation via high-temperature sintering, carbide formation and catalyst oxidation.

$$\frac{da}{dt} = -k_{\text{deact}} p_{\text{H}_2\text{O}}^\gamma a^n; n = 2 \text{ and } \gamma = 1 \quad (36)$$

The deactivation order, $n = 2$, was found to explain the catalyst deactivation in a study by Argyle and Bartholomew⁵⁸ while Khorashadizadeh and Atashi⁵⁹ found the order to be between 1 and 2 ($1 < n < 2$). For the sake of simplicity, $n = 2$ was chosen in the deactivation model fitting. In the case of water effect on the catalyst deactivation, this study proposes that water enhanced catalyst deactivation occurs via formation of the cobalt oxides (II) in presence of water as shown in Equation (37). Since the deactivation proposed here is of the first order with respect to water, $\gamma = 1$ is proposed to incorporate the enhanced catalyst deactivation in presence of water.



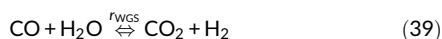
Assuming quasi-steady state was achieved during experimental runs, the algebraic form of Equation (36) can be derived, as shown in Equation (38).

$$a(t) = \frac{a_0}{1 + a_0 k_{\text{deact}} \Delta t p_{\text{H}_2\text{O}}^\gamma(t)}; a(t=0) = 1 \quad (38)$$

The quasi-steady state fails to capture the variation within the operating period for an experimental condition; however, the deviations are insignificant in comparison to variations between experimental points.

2.6 | The water gas shift reaction

The cobalt catalyst has very little water gas shift activity, but there are some CO_2 formed in the FTS in various amount. It is observed experimentally that CO_2 selectivity increases with the partial pressure of water^{34,57} and decreases with H_2/CO ratio.³⁴ The formation of CO_2 even though cobalt catalyst being WGS inactive is associated with Co(II)O formed due to the oxidation of the Co catalyst, which acts as the site for the WGS reaction.³⁴ A simple rate equation (Equations (40–42)) formulated by Moe,⁶⁰ which considers how far the current state is from the equilibrium state in water gas synthesis, is considered for the modeling of CO_2 formation via water gas shift reaction in the FTS.



$$r_{\text{WGS}} = k_{\text{CO}_2} \left(p_{\text{CO}} p_{\text{H}_2\text{O}} - \frac{1}{K_{\text{eq}}} p_{\text{CO}_2} p_{\text{H}_2} \right) \quad (40)$$

$$k_{\text{CO}_2} = k_{\text{WGS}} e^{-\frac{47400}{R_j k}} \quad (41)$$

$$K_{\text{eq}} = e^{\frac{45578}{R_j k} - 4.33} \quad (42)$$

3 | METHODS

3.1 | Kinetic experiment design and data

Fischer–Tropsch synthesis experiments were performed in a lab-scale fixed-bed reactor over a 20%Co/0.5Re $\gamma\text{-Al}_2\text{O}_3$ commercial catalyst. The lab reactor used in the test was of 1 cm diameter and 20 cm length. The experimental design superset consisted of two different temperature levels: 210 and 230°C and five distinct levels of H_2/CO ratio ranging from 1.12 to 2.55 at 2 MPa. For each design superset, experiments were carried out at a wide range of conversion level (10%–75%) with several catalysts to feed ratios without water in the feed, and additional points with 0.2 MPa water (total pressure increased to 2.2 MPa) in the feed. Each experimental state was maintained approximately for 24 h to achieve a steady state. The fresh catalyst was loaded after a considerable drop in the site time yield; altogether, the fresh catalyst was loaded 11 times, and average catalyst usage in the reactor was 150 – 500 h. The product gas was analyzed in a GC to measure the composition of CO , CO_2 , CH_4 , C_2H_4 , C_2H_6 , C_3H_6 , C_3H_8 , C_4H_8 , C_4H_{10} of the product gas. Altogether, 105 data points were obtained and applied for kinetic modeling. Further details on the kinetic study can be found elsewhere.^{7,61,62}

3.2 | Reactor model

The lab reactor was modeled as an isothermal plug flow reactor, and a set of species mass balance equations was solved using ordinary differential equation solver in the MATLAB. Here, ω_j is the mass fraction, R_j is the rate of formation, and M_j is the molecular weight of the species j , and \dot{W} is the total mass flow through the reactor.

$$\dot{W} \frac{d\omega_j}{dx} = R_j M_j m_{\text{cat}} \quad (43)$$

The temperature rise in the reactor was found to vary negligibly in the process. Furthermore, activation energy was estimated to 92.0 kJ/mol, which is comparable to literature published values.^{13,14,27} It indicates that the process has kinetic limitations, not diffusion limitations; thus, the lab reactor was modeled as a homogeneous plug flow reactor.

3.3 | Non-linear parameter optimization

The weighted non-linear least square minimizing weighted least square of error function as shown in Equation (44) with appropriate weights ($w_{i,j}$) along with relevant statistical analysis tools were used

Symbol	Description	Symbol	Description
X_{CO}	CO conversion [%]	S_{C_3P}	Selectivity to propane [%]
S_{CH_4}	Selectivity to CH_4 [%]	S_{C_4O}	Selectivity to butene [%]
S_{C_2O}	Selectivity to ethylene [%]	S_{C_4P}	Selectivity to butane [%]
S_{C_2P}	Selectivity to ethane [%]	$S_{C_{5+}}$	Selectivity to the lumps (C_{5+}) [%]
S_{C_3O}	Selectivity to propene [%]	S_{CO_2}	Selectivity to CO_2 [%]

TABLE 1 List of responses considered for the nonlinear model fitting

TABLE 2 Parameters and confidence interval of the fitted parameters

Parameter ($\hat{\theta}$)	Unit	Estimated Values	95% Confidence interval
<i>Main CO consumption rate equation (r_{FT})</i>			
Rate constant at $T_k = 483K$, (k_{ref})	$[kmol kg_{cat}^{-1} h^{-1} MPa^{-1.5}]$	7.05	(not estimated)
Activation energy (E_a^k)	$[kJ mol^{-1}]$	92.0	± 2.86
<i>Adsorption coefficients</i>			
a'	$[MPa^{-1}]$	12.0	± 0.600
b	$[MPa^{-0.5}]$	1.10	± 0.290
f'	$[MPa^{-1}]$	1.25	± 0.550
<i>Product distribution parameters (α and β model)</i>			
Kinetic constant for α -model at $T_k = 483K$, ($k_{\alpha,ref}$)	$[MPa]$	0.118	$\pm 5.90 \times 10^{-3}$
Activation energy ($E_a^{k_\alpha}$)	$[kJ mol^{-1}]$	4.77	± 2.81
Exponent for CO (z)	–	0.170	± 0.070
Exponent for $p_{H_2O}(y)$	–	0.095	± 0.017
Kinetic constant for β -model at $T_k = 483K$, ($k_{\beta,ref}$)	$[MPa]$	0.114	± 0.016
Activation energy, β -model ($E_a^{k_\beta}$)	$[kJ mol^{-1}]$	42.7	± 12.2
<i>Other parameters</i>			
Methanation reaction ratio (k_{CH_4})	[-]	6.38	± 0.62
Rate constant for ethylene hydrogenation reaction, ($k_{C_2H_4-C_2H_6}$)	[-]	0.27	± 0.17
Rate constant for ethylene conversion to higher olefin reaction ($k_{C_2H_4-olf}$)	[-]	0.67	± 0.17
Rate constant, WGS (k_{WGS})	$[kmol kg_{cat}^{-1} h^{-1} MPa^{-1}]$	119.1	± 16.1
Deactivation constant, (k_{deact})	$[h^{-1} MPa^{-1}]$	1.64×10^{-2}	$\pm 2.03 \times 10^{-3}$

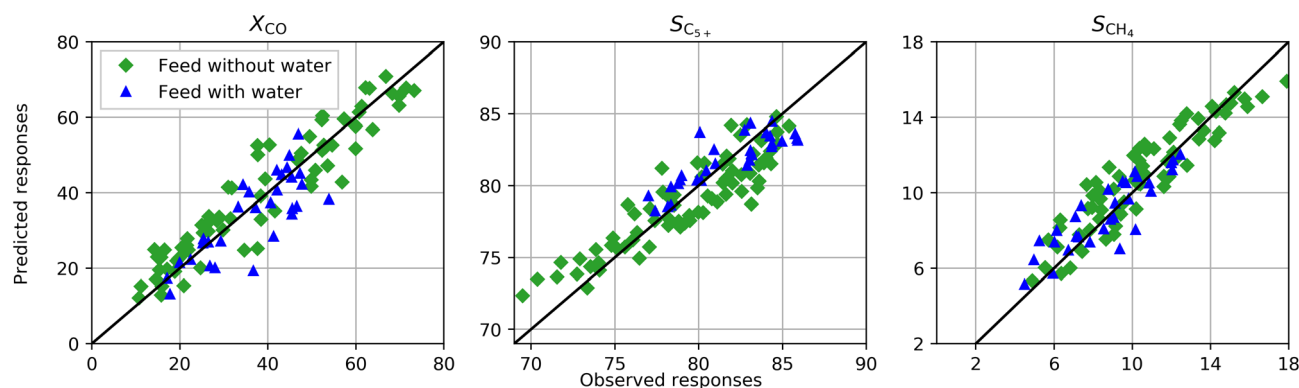


FIGURE 3 Parity plot of the primary responses over the wide range of experimental conditions [Color figure can be viewed at wileyonlinelibrary.com]

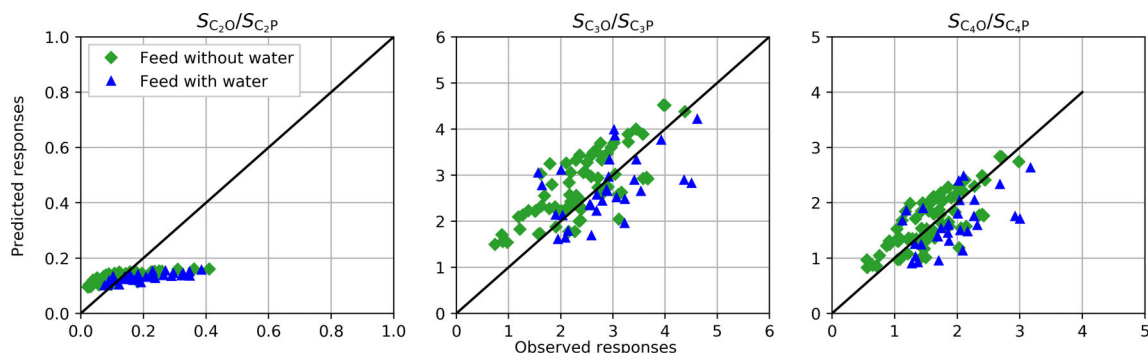


FIGURE 4 Parity plot of the olefins to paraffin ratio (C_2 – C_4) over the wide range of experimental conditions [Color figure can be viewed at wileyonlinelibrary.com]

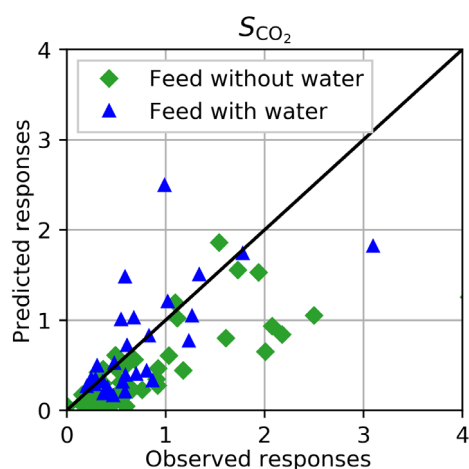


FIGURE 5 Parity plot of the CO_2 in the FTS over the wide range of experimental condition [Color figure can be viewed at wileyonlinelibrary.com]

$$S_{C_j} = \frac{F_{C_j, \text{out}} - F_{C_j, \text{in}}}{F_{CO_2, \text{in}} - F_{CO_2, \text{out}}} \times j \times 100 \quad (45)$$

The selectivity to CO_2 and lump C_{5+} and was calculated, as shown in Equations (46) and (47).

$$S_{CO_2} = \frac{F_{CO_2, \text{out}} - F_{CO_2, \text{in}}}{F_{CO_2, \text{in}} - F_{CO_2, \text{out}}} \times 100 \quad (46)$$

$$S_{C_{5+}} = 100 - \sum_{j=1}^4 S_{C_j}^P - \sum_{j=2}^4 S_{C_j}^O - S_{CO_2} \quad (47)$$

Besides, the mean absolute relative deviation (MARR) and root mean square error (RMSE) were also calculated to discriminate the model performance with the literature published model. The fitted parameters were normalized to avoid numerical problems such as rank deficiency of the gradient matrix and covariances between parameters.

$$MARR_j = \frac{1}{N_{\text{data}}} \sum_{i=1}^{N_{\text{data}}} \frac{|Y_{ij} - \hat{Y}_{ij}|}{Y_{ij}} \quad (48)$$

$$RMSE_j = \sqrt{\frac{1}{N_{\text{data}} - N_{\text{par}}} \sum_{i=1}^{N_{\text{data}}} (Y_{ij} - \hat{Y}_{ij})^2} \quad (49)$$

for determining optimal parameter values. The three significant responses, X_{CO} , $S_{C_{5+}}$, and S_{CH_4} , were prioritized while assigning weights. The parameters were normalized to ensure that the gradient matrix has a full rank. The marginal confidence intervals of the parameter were determined from the Hessian matrix at the optimal point to verify the significance of the fitted parameters.

$$WLSQ: \hat{\theta} = \arg \min_{\theta} \sum_{i=1}^{N_{\text{data}}} \sum_{j=1}^{N_{\text{resp}}} w_{ij} (Y_{ij} - \hat{Y}_{ij}(\theta))^2 \quad (44)$$

The conversion of CO , selectivities of individual components C_1 – C_4 paraffins, and C_2 – C_4 olefins, a C_{5+} lump and CO_2 were fitted as observed responses in the non-linear parameter estimation. The list of fitted responses is summarized in Table 1.

The selectivities to C_1 – C_4 , both paraffins and olefins, were calculated, as shown in Equation (45).

4 | RESULTS AND DISCUSSION

4.1 | Model fitting and evaluation of model fit

The estimated parameters, along with the confidence intervals of the estimated parameters, are presented in Table 2. The confidence interval for k_{ref} was not determined due to the strong correlation with adsorption coefficients. The confidence interval of the parameter shows that all the parameters are statistically significant. The sign of the fitted parameters is consistent with the physical laws and can be meaningfully used to describe FT kinetics and product distribution.

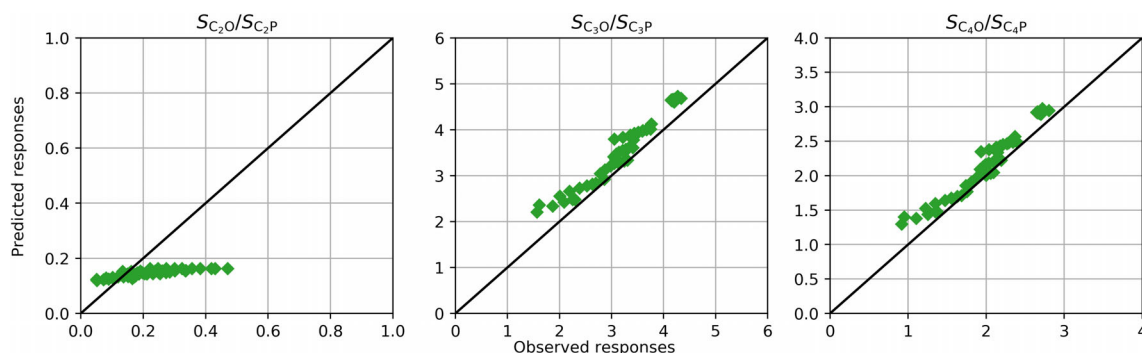


FIGURE 6 Parity plot of the olefins to paraffin ratio (C_2 – C_4) when the model is validated against the test dataset [Color figure can be viewed at [wileyonlinelibrary.com](#)]

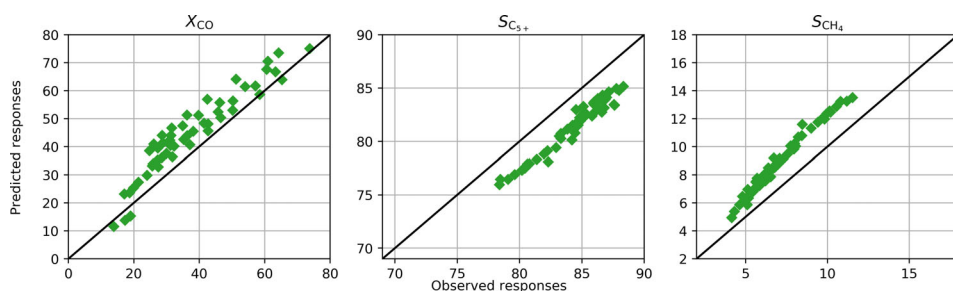


FIGURE 7 Parity plot of X_{CO} , $S_{C_{5+}}$, and S_{CH_4} when the model is validated against the test dataset [Color figure can be viewed at [wileyonlinelibrary.com](#)]

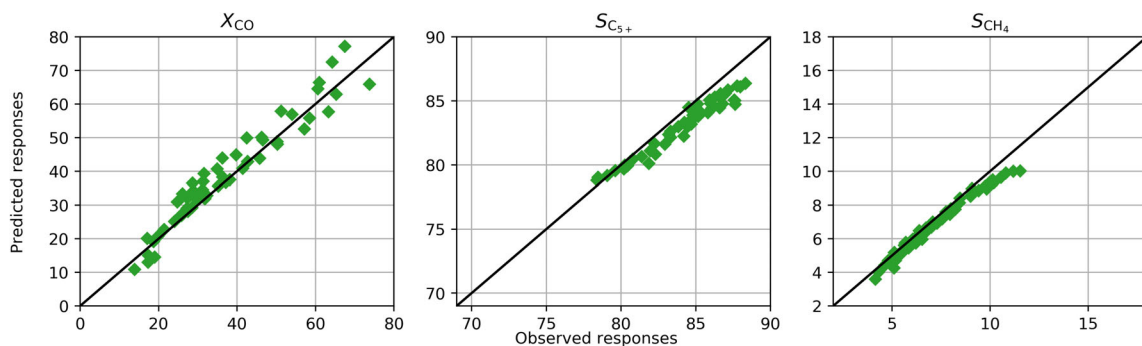


FIGURE 8 Parity plot of X_{CO} , $S_{C_{5+}}$, and S_{CH_4} when cross validated against the test dataset with selective parameter optimization [Color figure can be viewed at [wileyonlinelibrary.com](#)]

TABLE 3 Comparison of the activation energies for the proposed model and literature published values

Parameter	Proposed model	Literature
E_a^k	92 kJ/mol	104 kJ/mol ²⁷ 93 kJ/mol ^{13,14} 50 kJ/mol ⁶⁵
$E_a^{k_u}$	4.8 kJ/mol	16.8 kJ/mol ^{13,14} 16.3 kJ/mol ³⁶

The MARR values for overall responses was 23.1% which is comparable to the values reported by Todic et al (23.3%),^{13,14} Sonal et al⁴¹ (<20%), Koo et al (<20%),⁶³ and Abbasi et al⁶⁴ (<20%) and much better than the values of 48.4% reported by Ghouri et al.⁶⁵ The MARR value for CO conversion was 15.9% which is better than reported by Todic et al (18%).^{13,14} A much better fit with MARR = 5.9% for the overall

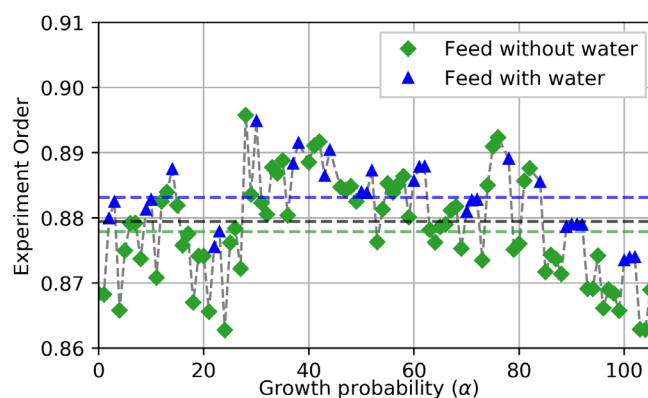


FIGURE 9 Growth probability (α) predicted by the fitted model at the outlet of the lab-reactor. Here, blue, green and black dotted lines represent the mean α for feed with water, without water and overall, respectively [Color figure can be viewed at [wileyonlinelibrary.com](#)]

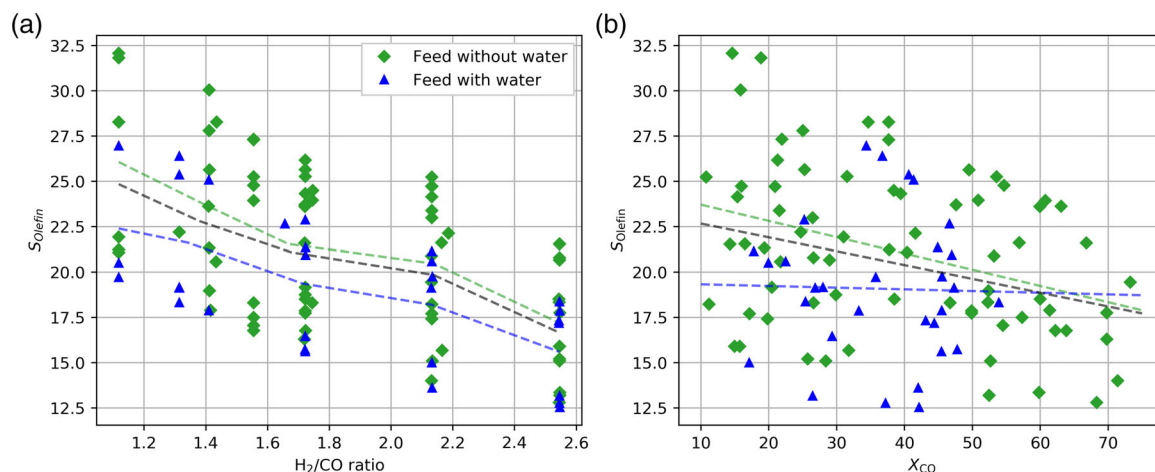


FIGURE 10 Here, (A) shows total selectivity to olefins (S_{olefin}) varying with H_2/CO ratio for feed with and without water. The blue, green and black dotted lines show trends of the means of the S_{olefin} at the particular H_2/CO ratio for feed with water, without water and overall, respectively. (B) shows S_{olefin} varying with X_{CO} for feed with and without water. The blue, green and black dotted lines show linear interpolation of S_{olefin} for feed with water, without water and overall, respectively (see text for detailed interpretation) [Color figure can be viewed at wileyonlinelibrary.com]

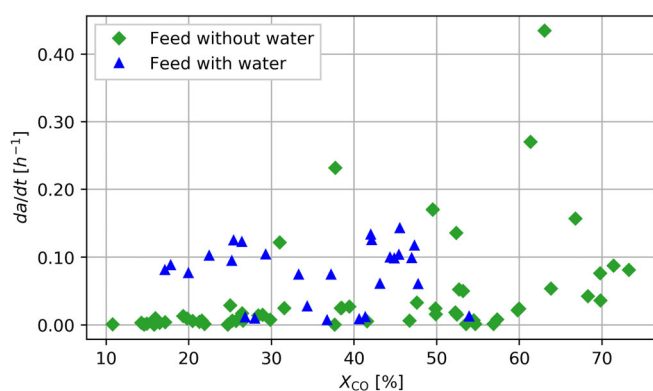


FIGURE 11 Characteristics of catalyst deactivation rate ($\frac{da}{dt}$) in the FTS over a cobalt catalyst [Color figure can be viewed at wileyonlinelibrary.com]

responses was reported by Moazami et al¹⁵ on their comprehensive FT kinetic modeling. Still, the fitted parameters and number of data points were identical, which might have resulted in model overfitting. The RMSE values for the fitted responses for X_{CO} , $S_{C_{5+}}$, and S_{CH_4} were 6.96%, 1.90%, and 1.30%, respectively. The estimated MARR and RMSE values for individual responses can be found in the Supporting Information.

The model was further evaluated using parity plots of all the responses with a specific focus on significant responses: X_{CO} , $S_{C_{5+}}$, and S_{CH_4} , as shown in Figure 3. Effect of water on the FTS, negative effect on the CO conversion⁷ and lower methane selectivities or high C_{5+} selectivities,^{13,14,36} are well described by the model. Overall, the model was able to predict X_{CO} , $S_{C_{5+}}$, S_{CH_4} , and $C_3 - C_4$ olefins to paraffins ratios, Figure 4, reasonably well with the uniform error deviation. In the case of ethylene to ethane ratio, the predicted selectivities were considered acceptable as ethylene is present in very low quantity which is well within the range of sensitivity of the laboratory

equipment, thus, it is possible that the error was propagated from the experimental selectivities to the predicted. Besides, the primary focus of FT modeling was to develop highly predictive model for the key response, X_{CO} , $S_{C_{5+}}$, and S_{CH_4} , which is critical for the FT reactor modeling and optimization for the design and scale-up of the BTL plants.

In the case of modeling of CO_2 formation in the FTS, Figure 5 shows that the model can predict CO_2 selectivity reasonably well, specifically at extreme process conditions, specifically at low H_2/CO ratio and higher partial pressure of water in the stream, while at the same time maintaining acceptable predictability for key responses.

4.2 | Cross-validation of the fitted model

The fitted model was cross-validated against a test dataset from the FTS experiments over the cobalt catalysts by Lillebo et al.⁶⁶ The experiments had a comparable setup: identical reactor configuration, a comparable catalyst to support ratio and physical characteristics; although catalysts were not identical. The process conditions for test dataset were temperature = 210°C, pressure = 2 MPa, feed H_2/CO ratio = 1.1–2.55, and conversion level = 10%–80% (obtained by varying feed to catalyst ratio). The MARR values of the overall responses when the fitted model was cross-validated against test data were 23.0% and the RMSEs for X_{CO} , $S_{C_{5+}}$, and S_{CH_4} were 8.71%, 1.94%, and 3.01%, respectively. The parity plot for $C_3 - C_4$ olefins and $C_3 - C_4$ paraffins, Figure 6, shows that the model performs reasonably well against the test data. In the case of ethylene to ethane ratio, the cross-validated model fit is considered acceptable due to similar reasons as described in the case of experimental data used in the model fitting.

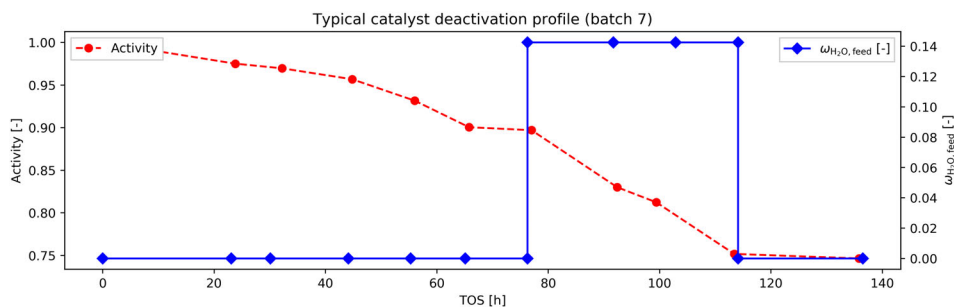


FIGURE 12 Catalyst deactivation as a function of the partial pressure of water in the feed [Color figure can be viewed at wileyonlinelibrary.com]

The parity plot of X_{CO} , $S_{C_{5+}}$, and S_{CH_4} , Figure 7, shows that there are systematic biases that can be associated with the differences in catalyst properties such as higher site activity as well as a higher tendency toward methanation for the catalyst used in the generation of fitted data in comparison to the catalyst in the test data.

These catalyst specific systematic biases can be addressed by optimizing methanation ratio (k_{CH_4}) and reference kinetic rate constant (k_{ref}) for test data without much change in model structure and fitted parameter values, as shown in Figure 8. The MARR value improved from 23.0 to 21.2% for overall responses, and 23.7 to 9.9% for CO conversion with selective optimization of the key parameters which also indicates that the model structure performs reasonably well against test data without much change in parameter values for different catalysts.

4.3 | Behavior of the fitted model

4.3.1 | Estimated parameters

The activation energy for the overall FT reaction (E_a^k) was estimated to be 92.0 kJ/mol, which is comparable to literature published values. Ma et al estimated activation energy to be 104 kJ/mol,²⁷ and Todic et al estimated to be 93 kJ/mol,^{13,14} while Ghouri et al estimated much lower activation energy of 50.7 kJ/mol,⁶⁵ while a wide range of activation energy (27–124 kJ/mol)³¹ were reported in the literature. In the case of growth probability, the activation energy for the growth probability ($E_a^{k_g}$) was estimated to be 4.8 kJ/mol which is much lower than estimated by Ostadi et al³⁶ (16.3 kJ/mol) and Todic et al^{13,14} (16.8 kJ/mol). Table 3 summarizes activation energies (E_a^k and $E_a^{k_g}$) for the proposed model and literature published values. The estimated exponent parameter values for α -model shows that the probability of formation of longer chain HC (increasing α) increases with p_{CO} and p_{H_2O} . The fitted model accurately captures anomalies in the FTS; the selectivity to methane is 5.38 times higher than the ideal distribution (i.e., methanation ratio, $k_{CH_4} = 6.38$), and selectivity to ethylene is 94% lower than the ideal distribution (i.e., $k_{C_2H_4-C_2H_6} + k_{C_2H_4-olf} = 0.94$).

4.3.2 | Growth probability and olefin-paraffin distribution

The plot of growth probability at the outlet of the reactor is shown in Figure 9. It shows that the growth probability for the feed with 10 vol

% water is higher than for the feed without water for comparable H_2/CO ratio, conversion level and other process condition. The model predicts that C_{5+} selectivity increases while lower chain hydrocarbon production decreases with feed water addition, which is also widely reported in the literature.^{37,49,57,67}

Figure 10 shows the total selectivity to olefins (S_{olefin}) predicted by the fitted model at the experimental conditions. A clear negative impact of H_2/CO ratio and CO conversion on the olefins fraction is predicted by the model, which is in agreement with the literature.^{22,34} The fitted model predicts that water addition has a small negative impact on the selectivity to olefins, which is in direct contradiction to the positive effect of water reported in the literature.⁶⁸ This disagreement arises mainly because H_2/CO ratio and residence time represented in terms of CO conversion has a much more dominant effect on the olefins selectivities and outweighs the impact of any other factors.

4.3.3 | Catalyst deactivation

Figures 11 and 12 show a predicted deactivation rate as a function of CO conversion and water addition in the feed. The deactivation rate is most pronounced with the water addition on the feed, as seen in Figure 12, or at higher conversion, as seen in Figure 11, indicating that indigenous water or extra water added in the feed contributes to the enhanced deactivation of the cobalt catalyst. Overall, the deactivation model performed reasonably well as the model can predict the CO consumption over a wide range of process condition and explain enhanced catalyst deactivation in the presence of water.

5 | CONCLUSION

A detailed kinetic model structure based on the H_2 -assisted CO dissociation mechanism and novel product distribution modeling was developed for the FTS over a 20%Co/0.5Re γ - Al_2O_3 commercial catalyst. The parameters were estimated against a set of experimental data from the kinetic studies on an experimental fixed bed lab reactor encompassing a wide range of experimental variations: the pressure of 2.0–2.2 MPa, the temperature of 210–230°C, conversion range of 10%–75% and feed with/without water and were validated against test data from the similar reactor setup. The estimated parameters are closely aligned with the literature reported parameter values and

physical interpretation. The mean absolute relative deviation value is 23.3%, which is comparable to the values reported in the literature. The predictive model can accurately address some of the recent experimental pieces of evidences overlooked in the contemporary FTS kinetic modeling approaches; effect of water on the CO consumption rate and growth probability, growth probability independent of the hydrogen partial pressure, anomalies in the FTS and olefin-paraffin distribution. Besides, the model can be used to mechanistically investigate the effect of process variations, specifically the effect of water, syngas composition, temperature and pressure, on the FTS process modeling.

NOTATION

SYMBOLS

a', b	adsorption coefficients in the primary FT reactions
f, K	[MPa ^{-m}], m is the sum of exponents of partial pressure
a_0	catalyst activity at $t = t_0$ [-]
B	olefins rate fraction [-]
E_a	activation energy [kJ/mol]
F_i	molar flow of component i [kmol/h]
F_{C_j}	molar flow of component with j number of carbons [kmol/h]
k	kinetic constant [kmol g _{cat} ⁻¹ h ⁻¹ MPa ^{-q}], q is sum of exponents of the partial pressures
k_i	kinetic constant [MPa ⁻ⁿ], n is sum of exponents of the partial pressures
k_{WGS}	rate constant of water gas shift reaction [kmol g _{cat} ⁻¹ h ⁻¹ Mpa ⁻²]
M_i	molecular weight of component i [kg/kmol]
N_i	number of carbon atoms in the component i [-]
p	pressure [MPa]
p_i	partial pressure of component i [MPa]
r_i	CO consumption rate [kmol kg _{cat} ⁻¹ h ⁻¹]
S_i	selectivity to component i [%]
T_k	temperature in the reactor [K]
R	universal gas constant [kJ K ⁻¹ kmol ⁻¹]
t	time on stream [h]
U	hydrogen utilization ratio [-]
\dot{W}	mass flow rate [kg s ⁻¹]
x	dimensionless reactor length [-]
X_{CO}	CO conversion [%]
y	exponent for H ₂ O in growth model [-]
Y_i	observed responses [%]
\hat{Y}_i	predicted or estimated responses [%]
z	exponent for CO in growth model [-]

Acronyms

ASF	Anderson-Schultz-Flory distribution
BtL	biomass to liquids
CtL	coal to liquids
FT	Fischer-Tropsch
FTS	Fischer-Tropsch synthesis
GtL	gas to liquids

HTFT	high temperature Fischer-Tropsch
LHHW	Langmuir-Hinshelwood-Hougen-Watson
LTFT	low temperature Fischer-Tropsch
MARR	mean absolute relative residuals
RMSE	root mean square error
WGS	water gas shift reaction

Greek symbol

α	growth probability [-]
β	parameter of olefin-paraffin distribution [-]
θ	regression parameter [-]
ν_i	stoichiometric coefficient of component i [-]
ω_i	mass fraction of component i [-]

AUTHOR CONTRIBUTIONS

Umesh Pandey: Data curation; formal analysis; investigation; methodology; resources; software; validation; visualization; writing-original draft; writing-review and editing. **Anders Runningen:** Data curation. **Ljubiša Gavrilović:** Data curation; formal analysis; investigation. **Erik Jørgensen:** Data curation. **Koteswara Putta:** Data curation. **Kumar Rout:** Data curation; funding acquisition; writing-review and editing. **Erling Rytter:** Conceptualization; data curation; formal analysis; investigation; writing-review and editing. **Edd Blekkan:** Data curation; formal analysis; investigation; project administration; supervision; validation; writing-original draft. **Magne Hillestad:** Conceptualization; data curation; formal analysis; investigation; methodology; supervision; validation; writing-review and editing.

DATA AVAILABILITY STATEMENT

Data are available on request from the authors.

ORCID

Magne Hillestad  <https://orcid.org/0000-0001-5658-8120>

REFERENCES

- United States. Bureau of Mines, Anderson R. *Physical Chemistry of the Fischer-Tropsch Synthesis*. Washington DC: Bureau of Mines; 1959.
- van Santen RA, Markvoort AJ, Filot IAW, Ghouri MM, Hensen EJM. Mechanism and microkinetics of the Fischer-Tropsch reaction. *Phys Chem Chem Phys*. 2013;15(40):17038-17063. <https://doi.org/10.1039/C3CP52506F>.
- Dry ME. The Fischer-Tropsch process—commercial aspects. *Catal Today*. 1990;6(3):183-206. [https://doi.org/10.1016/0920-5861\(90\)85002-6](https://doi.org/10.1016/0920-5861(90)85002-6).
- Dry ME. The Fischer-Tropsch process: 1950–2000. *Catal Today*. 2002;71(3):227-241. [https://doi.org/10.1016/S0920-5861\(01\)00453-9](https://doi.org/10.1016/S0920-5861(01)00453-9).
- Outi A, Rautavuoma I, van der Baan HS. Kinetics and mechanism of the fischer tropsch hydrocarbon synthesis on a cobalt on alumina catalyst. *Appl Catal*. 1981;1(5):247-272. [https://doi.org/10.1016/0166-9834\(81\)80031-0](https://doi.org/10.1016/0166-9834(81)80031-0).
- Wilhelm DJ, Simbeck DR, Karp AD, Dickenson RL. Syngas production for gas-to-liquids applications: technologies, issues and outlook. *Fuel Process Technol*. 2001;71(1):139-148. [https://doi.org/10.1016/S0378-3820\(01\)00140-0](https://doi.org/10.1016/S0378-3820(01)00140-0).
- Rytter E, Holmen A. Consorted vinylene mechanism for cobalt Fischer-Tropsch synthesis encompassing water or hydroxyl assisted

- CO-activation. *Top Catal.* 2018;61(9):1024-1034. <https://doi.org/10.1007/s11244-018-0932-3>.
8. Sarup B, Wojciechowski BW. Studies of the Fischer-Tropsch synthesis on a cobalt catalyst II. Kinetics of carbon monoxide conversion to methane and to higher hydrocarbons. *Can J Chem Eng.* 1989;67(1):62-74. <https://doi.org/10.1002/cjce.5450670110>.
 9. Wojciechowski BW. The kinetics of the Fischer-Tropsch synthesis. *Catal Rev.* 1988;30(4):629-702. <https://doi.org/10.1080/01614948808071755>.
 10. Iglesia E, Reyes SC, Madon RJ, Soled SL. Selectivity control and catalyst design in the Fischer-Tropsch synthesis: sites, pellets, and reactors. In: Eley DD, Pines H, Weisz PB, eds. *Advances in Catalysis*. Vol 39. Cambridge, Massachusetts: Academic Press; 1993:221-302. [https://doi.org/10.1016/S0360-0564\(08\)60579-9](https://doi.org/10.1016/S0360-0564(08)60579-9).
 11. Atashi H, Siami F, Mirzaei AA, Sarkari M. Kinetic study of Fischer-Tropsch process on titania-supported cobalt-manganese catalyst. *J Ind Eng Chem.* 2010;16(6):952-961. <https://doi.org/10.1016/j.jiec.2010.04.005>.
 12. Keyvanloo K, Lanham SJ, Hecker WC. Kinetics of Fischer-Tropsch synthesis on supported cobalt: effect of temperature on CO and H₂ partial pressure dependencies. *Catal Today.* 2016;270:9-18. <https://doi.org/10.1016/j.cattod.2016.03.019>.
 13. Todic B, Ma W, Jacobs G, Davis BH, Bukur DB. CO-insertion mechanism based kinetic model of the Fischer-Tropsch synthesis reaction over Re-promoted Co catalyst. *Catal Today.* 2014;228:32-39. <https://doi.org/10.1016/j.cattod.2013.08.008>.
 14. Todic B, Ma W, Jacobs G, Davis BH, Bukur DB. Corrigendum to: CO-insertion mechanism based kinetic model of the Fischer-Tropsch synthesis reaction over re-promoted Co catalyst. *Catal Today.* 2015;242:386. <https://doi.org/10.1016/j.cattod.2014.08.020>.
 15. Moazami N, Wyszynski ML, Rahbar K, Tsolakis A, Mahmoudi H. A comprehensive study of kinetics mechanism of Fischer-Tropsch synthesis over cobalt-based catalyst. *Chem Eng Sci.* 2017;171:32-60. <https://doi.org/10.1016/j.ces.2017.05.022>.
 16. Storsæter S, Chen D, Holmen A. Mikrokinetic modelling of the formation of C1 and C2 products in the Fischer-Tropsch synthesis over cobalt catalysts. *Surf Sci.* 2006;600(10):2051-2063. <https://doi.org/10.1016/j.susc.2006.02.048>.
 17. Visconti CG, Tronconi E, Lietti L, Forzatti P, Rossini S, Zennaro R. Detailed kinetics of the Fischer-Tropsch synthesis on cobalt catalysts based on H-assisted CO activation. *Top Catal.* 2011;54(13):786-800. <https://doi.org/10.1007/s11244-011-9700-3>.
 18. Qi Y, Yang J, Chen D, Holmen A. Recent progresses in understanding of co-based Fischer-Tropsch catalysis by means of transient kinetic studies and theoretical analysis. *Catal Lett.* 2015;145(1):145-161. <https://doi.org/10.1007/s10562-014-1419-x>.
 19. Weller S, Hofer LJE, Anderson RB. The role of bulk cobalt carbide in the Fischer-Tropsch synthesis. *J Am Chem Soc.* 1948;70(2):799-801. <https://doi.org/10.1021/ja01182a108>.
 20. Shafer WD, Gnanamani MK, Graham UM, et al. Fischer-Tropsch: product selectivity—the fingerprint of synthetic fuels. *Catalysts.* 2019; 9(3):259. <https://doi.org/10.3390/catal9030259>.
 21. Zennaro R, Tagliabue M, Bartholomew CH. Kinetics of Fischer-Tropsch synthesis on titania-supported cobalt. *Catal Today.* 2000;58(4):309-319. [https://doi.org/10.1016/S0920-5861\(00\)00264-9](https://doi.org/10.1016/S0920-5861(00)00264-9).
 22. Pannell RB, Kibby CL, Kobylnski TP. A Steady-state study of Fischer-Tropsch product distributions over cobalt, iron and ruthenium. In: Seivama T, Tanabe K, eds. *Studies in Surface Science and Catalysis*. Vol 7. Amsterdam: New Horizons in Catalysis. Elsevier; 1981:447-459. [https://doi.org/10.1016/S0167-2991\(09\)60290-1](https://doi.org/10.1016/S0167-2991(09)60290-1).
 23. Yang C-H, Massoth FE, Oblad AG. Kinetics of CO+H₂ reaction over Co-Cu-Al₂O₃ catalyst. In: Kugler EL, Steffgen FW, eds. *Hydrocarbon Synthesis from Carbon Monoxide and Hydrogen*. Vol 178. Washington DC: Advances in Chemistry. American Chemical Society; 1979:35-46. <https://doi.org/10.1021/ba-1979-0178.ch005>.
 24. Yates IC, Satterfield CN. Intrinsic kinetics of the Fischer-Tropsch synthesis on a cobalt catalyst. *Energy Fuel.* 1991;5(1):168-173. <https://doi.org/10.1021/ef00025a029>.
 25. Bhatelia T, Li C, Sun Y, Hazewinkel P, Burke N, Sage V. Chain length dependent olefin re-adsorption model for Fischer-Tropsch synthesis over Co-Al₂O₃ catalyst. *Fuel Process Technol.* 2014;125:277-289. <https://doi.org/10.1016/j.fuproc.2014.03.028>.
 26. Das TK, Conner WA, Li J, Jacobs G, Dry ME, Davis BH. Fischer-Tropsch synthesis: kinetics and effect of water for a Co/SiO₂ catalyst. *Energy Fuel.* 2005;19(4):1430-1439. <https://doi.org/10.1021/ef049869j>.
 27. Ma W, Jacobs G, Sparks DE, et al. Fischer-Tropsch synthesis: kinetics and water effect study over 25%Co/Al₂O₃ catalysts. *Catal Today.* 2014;228:158-166. <https://doi.org/10.1016/j.cattod.2013.10.014>.
 28. Van Steen E, Schulz H. Polymerisation kinetics of the Fischer-Tropsch CO hydrogenation using iron and cobalt based catalysts. *Appl Catal Gen.* 1999;186(1):309-320. [https://doi.org/10.1016/S0926-860X\(99\)00151-9](https://doi.org/10.1016/S0926-860X(99)00151-9).
 29. Withers HP, Eliezer KF, Mitchell JW. Slurry-phase Fischer-Tropsch synthesis and kinetic studies over supported cobalt carbonyl derived catalysts. *Ind Eng Chem Res.* 1990;29(9):1807-1814. <https://doi.org/10.1021/ie00105a011>.
 30. Sun Y, Yang G, Xu M, Xu J, Sun Z. A simple coupled ANNs-RSM approach in modeling product distribution of Fischer-Tropsch synthesis using a microchannel reactor with Ru-promoted Co/Al₂O₃ catalyst. *Int J Energy Res.* 2020;44(2):1046-1061. <https://doi.org/10.1002/er.4990>.
 31. Van Der Laan GP, AACM B. Kinetics and selectivity of the Fischer-Tropsch synthesis: a literature review. *Catal Rev.* 1999;41(3-4):255-318. <https://doi.org/10.1081/CR-100101170>.
 32. Vervloet D, Kapteijn F, Nijenhuis J, Ommen JR van. Fischer-Tropsch reaction-diffusion in a cobalt catalyst particle: aspects of activity and selectivity for a variable chain growth probability. *Cat Sci Technol* 2012;2(6):1221-1233. doi:<https://doi.org/10.1039/C2CY20060K>
 33. Kruit KD, Vervloet D, Kapteijn F, Ommen JR van. Selectivity of the Fischer-Tropsch process: deviations from single alpha product distribution explained by gradients in process conditions. *Cat Sci Technol* 2013;3(9):2210-2213. doi:<https://doi.org/10.1039/C3CY00080J>
 34. Holmen A, Rytter E. Perspectives on the effect of water in cobalt Fischer-Tropsch synthesis. *ACS Catal.* 2017;7(8):5321-5328. <https://doi.org/10.1021/acscatal.7b01525>.
 35. Oosterbeek H, van Bavel AP. Extended abstract 992. *11th Natural Gas Conversion Symposium, Tromsø*; 2016.
 36. Ostadi M, Rytter E, Hillestad M. Evaluation of kinetic models for Fischer-Tropsch cobalt catalysts in a plug flow reactor. *Chem Eng Res Des.* 2016;114:236-246. <https://doi.org/10.1016/j.cherd.2016.08.026>.
 37. Rytter E, Tsakoumis NE, Holmen A. On the selectivity to higher hydrocarbons in Co-based Fischer-Tropsch synthesis. *Catal Today.* 2016;261:3-16. <https://doi.org/10.1016/j.cattod.2015.09.020>.
 38. Filip L, Zámotný P, Rauch R. Mathematical model of Fischer-Tropsch synthesis using variable alpha-parameter to predict product distribution. *Fuel.* 2019;243:603-609. <https://doi.org/10.1016/j.fuel.2019.01.121>.
 39. Kuipers EW, Vinkenburg IH, Oosterbeek H. Chain length dependence of α -olefin Readsorption in Fischer-Tropsch synthesis. *J Catal.* 1995; 152(1):137-146. <https://doi.org/10.1006/jcat.1995.1068>.
 40. Snel R. Deviations of Fischer-Tropsch products from an Anderson-Schulz-Flory distribution. *Catal Lett.* 1988;1(10):327-330. <https://doi.org/10.1007/BF00774875>.
 41. Sonal PKK, Upadhyayula S. Detailed kinetics of Fischer Tropsch synthesis over Fe-Co bimetallic catalyst considering chain length dependent olefin desorption. *Fuel.* 2019;236:1263-1272:1263-1272. <https://doi.org/10.1016/j.fuel.2018.09.087>.

42. Todic B, Bhatelia T, Froment GF, et al. Kinetic model of Fischer-Tropsch synthesis in a slurry reactor on Co-Re/Al₂O₃ catalyst. *Ind Eng Chem Res.* 2013;52(2):669-679. <https://doi.org/10.1021/ie3028312>.
43. Schulz H. Major and minor reactions in Fischer-Tropsch synthesis on cobalt catalysts. *Top Catal.* 2003;26(1):73-85. <https://doi.org/10.1023/B:TOCA.0000012988.86378.21>.
44. Lee WH, Bartholomew CH. Multiple reaction states in CO hydrogenation on alumina-supported cobalt catalysts. *J Catal.* 1989;120(1):256-271. [https://doi.org/10.1016/0021-9517\(89\)90264-9](https://doi.org/10.1016/0021-9517(89)90264-9).
45. Friedel RA, Anderson RB. Composition of synthetic liquid fuels. I. Product distribution and analysis of C5-C8 paraffin isomers from cobalt catalyst. *J Am Chem Soc.* 1950;72(3):1212-1215. <https://doi.org/10.1021/ja01159a039>.
46. Huff GA, Satterfield CN. Evidence for two chain growth probabilities on iron catalysts in the Fischer-Tropsch synthesis. *J Catal.* 1984;85(2):370-379. [https://doi.org/10.1016/0021-9517\(84\)90226-4](https://doi.org/10.1016/0021-9517(84)90226-4).
47. Tau L-M, Dabbagh H, Bao S, Davis BH. Fischer-Tropsch synthesis. Evidence for two chain growth mechanisms. *Catal Lett.* 1991;7(1-4):127-140. <https://doi.org/10.1007/BF00764496>.
48. Hillestad M. Modeling the Fischer-Tropsch product distribution and model implementation. *Chem Product Process Model.* 2015;10(3):147-159. <https://doi.org/10.1515/cppm-2014-0031>.
49. Storsæter S, Borg Ø, Blekkan EA, Holmen A. Study of the effect of water on Fischer-Tropsch synthesis over supported cobalt catalysts. *J Catal.* 2005;231(2):405-419. <https://doi.org/10.1016/j.jcat.2005.01.036>.
50. Shi B, Davis BH. Fischer-Tropsch synthesis: the paraffin to olefin ratio as a function of carbon number. *Catal Today.* 2005;106(1):129-131. <https://doi.org/10.1016/j.cattod.2005.07.159>.
51. Yan F, Qian W, Sun Q, Zhang H, Ying W, Fang D. Product distributions and olefin-to-paraffin ratio over an iron-based catalyst for Fischer-Tropsch synthesis. *Reac Kinet Mech Cat.* 2014;113(2):471-485. <https://doi.org/10.1007/s11144-014-0746-7>.
52. Schulz H, Claeys M. Reactions of α -olefins of different chain length added during Fischer-Tropsch synthesis on a cobalt catalyst in a slurry reactor. *Appl Catal Gen.* 1999;186(1):71-90. [https://doi.org/10.1016/S0926-860X\(99\)00165-9](https://doi.org/10.1016/S0926-860X(99)00165-9).
53. Einbeigi A, Atashi H, Mirzaei AA, Zohdi-Fasaei H, Golestan S. Development of new comprehensive kinetic models for Fischer-Tropsch synthesis process over Fe-Co/ γ -Al₂O₃ nanocatalyst in a fixed-bed reactor. *J Taiwan Inst Chem Eng.* 2019;103:57-66. <https://doi.org/10.1016/j.jtice.2019.07.004>.
54. Rytter E, Yang J, Borg Ø, Holmen A. Significance of C3 olefin to paraffin ratio in cobalt Fischer-Tropsch synthesis. *Catalysts.* 2020;10(9):967. <https://doi.org/10.3390/catal10090967>.
55. Rytter E, Holmen A. On the support in cobalt Fischer-Tropsch synthesis—emphasis on alumina and aluminates. *Catal Today.* 2016;275:11-19. <https://doi.org/10.1016/j.cattod.2015.11.042>.
56. Tsakoumis NE, Rønning M, Borg Ø, Rytter E, Holmen A. Deactivation of cobalt based Fischer-Tropsch catalysts: a review. *Catal Today.* 2010;154(3):162-182. <https://doi.org/10.1016/j.cattod.2010.02.077>.
57. Dalai AK, Davis BH. Fischer-Tropsch synthesis: a review of water effects on the performances of unsupported and supported Co catalysts. *Appl Catal Gen.* 2008;348(1):1-15. <https://doi.org/10.1016/j.apcata.2008.06.021>.
58. Argyle MD, Bartholomew CH. Heterogeneous catalyst deactivation and regeneration: a review. *Catalysts.* 2015;5(1):145-269. <https://doi.org/10.3390/catal5010145>.
59. Khorashadzadeh M, Atashi H. Modeling the kinetics of cobalt Fischer-Tropsch catalyst deactivation trends through an innovative modified Weibull distribution. *Phys Chem Chem Phys.* 2017;19(29):19252-19261. <https://doi.org/10.1039/C7CP02210G>.
60. Moe JM. Design of water-gas shift reactors. *Chem Eng Prog.* 1962;58(3):33-36.
61. Borg Ø, Hammer N, Eri S, et al. Fischer-Tropsch synthesis over unpromoted and re-promoted γ -Al₂O₃ supported cobalt catalysts with different pore sizes. *Catal Today.* 2009;142(1):70-77. <https://doi.org/10.1016/j.cattod.2009.01.012>.
62. Gavrilović L, Jørgensen EA, Pandey U, et al. Fischer-Tropsch synthesis over an alumina-supported cobalt catalyst in a fixed bed reactor—effect of process parameters. *Catal Today.* 2020. <https://doi.org/10.1016/j.cattod.2020.07.055>.
63. Koo HM, Park MJ, Moon DJ, Bae JW. Kinetic models of Fischer-Tropsch synthesis reaction over granule-type Pt-promoted Co/Al₂O₃ catalyst. *Kor J Chem Eng.* 2018;35(6):1263-1273. <https://doi.org/10.1007/s11814-018-0032-x>.
64. Abbasi M, Mirzaei AA, Atashi H. The mechanism and kinetics study of Fischer-Tropsch reaction over iron-nickel-cerium nano-structure catalyst. *Int J Hydrogen Energy.* 2019;44(45):24667-24679. <https://doi.org/10.1016/j.ijhydene.2019.07.222>.
65. Ghouri MM, Afzal S, Hussain R, Blank J, Bukur DB, Elbashir NO. Multi-scale modeling of fixed-bed Fischer Tropsch reactor. *Comput Chem Eng.* 2016;91:38-48. <https://doi.org/10.1016/j.compchemeng.2016.03.035>.
66. Lillebø A, Rytter E, Blekkan EA, Holmen A. Fischer-Tropsch synthesis at high conversions on Al₂O₃-supported Co catalysts with different H₂/CO levels. *Ind Eng Chem Res.* 2017;56(45):13281-13286. <https://doi.org/10.1021/acs.iecr.7b01801>.
67. Borg Ø, Storsæter S, Eri S, Wigum H, Rytter E, Holmen A. The effect of water on the activity and selectivity for γ -alumina supported cobalt Fischer-Tropsch catalysts with different pore sizes. *Catal Lett.* 2006;107(1):95-102. <https://doi.org/10.1007/s10562-005-9736-8>.
68. Dalai AK, Das TK, Chaudhari KV, Jacobs G, Davis BH. Fischer-Tropsch synthesis: water effects on Co supported on narrow and wide-pore silica. *Appl Catal Gen.* 2005;289(2):135-142. <https://doi.org/10.1016/j.apcata.2005.04.045>.

SUPPORTING INFORMATION

Additional supporting information may be found online in the Supporting Information section at the end of this article.

How to cite this article: Pandey U, Runningen A, Gavrilović L, et al. Modeling Fischer-Tropsch kinetics and product distribution over a cobalt catalyst. *AIChE J.* 2021;67:e17234. <https://doi.org/10.1002/aic.17234>